Thermal properties of Na_2O–P_2O_5–Fe_2O_3 polyphosphate glasses

Paweł Goj[1] · Małgorzata Ciecińska[1] · Magdalena Szumera[1] · Paweł Stoch[1]

Abstract

Iron phosphate glasses are materials that can have many applications like durable matrixes in waste immobilization techniques, biomaterials, optoelectronic devices, etc. Their possible usage is related to their glass network and thermal properties. The influence of Na_2O content on thermal properties and crystallization ability of iron phosphate glass of base composition 30 Fe_2O_3–70 P_2O_5 mol% were studied. Increasing the content of Na_2O causes a decrease in transformation temperature and increase in ΔC_p. Characteristic temperatures, thermal stability and crystallizing phases were determined. Increasing content of sodium causes depolarization of iron phosphate glass network which causes a continuous change in ΔC_p and glass transformation temperature. Discontinuous change in some glass properties suggests structure rebuilding about 30 mol% of Na_2O.

Keywords Phosphate glasses · Glass crystallization · DSC/TG analysis · Raman spectroscopy

Introduction

Iron phosphate glasses are a group of materials which possess very interesting properties. They can have very high chemical durability which makes them a good candidate to be considered as materials for vitrifying dangerous waste. Due to the presence of phosphorous, they can be biocompatible and may be used as corrosion-resistant materials for bone implants [1–8].

Generally, phosphate glasses have lower transformation temperature, higher thermal expansion coefficient than silicate and also high radiation resistance [9–15]. Unfortunately, their possible application may be strongly limited because of the occurrence of easily hydrated P–O–P bridges. The effect is being strongly reduced by substitution of the bridges by much more chemical-resistant P–O–Fe linkages. Thus, materials of superior chemical resistance can be obtained [16, 17]. As such, the highest chemical durability is achieved for the composition 60 P_2O_5–40 Fe_2O_3 mol% [13]. Further increase in iron concentration in the glass leads to partial crystallization of the melt [18]. Iron phosphate glasses except excellent chemical resistance are able to accept their network higher concentrations of species in which solubility is strongly reduced in silicate glasses like sulfates and chlorides. The species due to the effect of liquation may precipitate as separate phases during cooling [3–5, 19]. Furthermore, iron phosphate glasses have a melting temperature of 100–200 K lower than borosilicate and lower viscosity of the melt. Therefore, waste vitrification temperature can be lower and homogenization time can be shorter, resulting in limited evaporation of waste volatile components such as Cs or Ru [9, 12, 20]. This also gives a possibility to use the glasses in many ceramic processes where temperature needs to be limited.

Because glass is a metastable material, very important factors are thermal stability parameters, e.g., Angell parameter. They describe the stability of glasses against the crystallization of the melts. Thus, they can be helpful in designing conditions of production of glass–ceramic materials or homogenous glass [21, 22]. Iron phosphate glasses with Fe_2O_3 content up to about 40 mol% have good thermal stability comparable with silicate glasses, and over this value, the stability decreases and partial crystallization can take place [3, 23, 24].

In the glasses, both Fe(II) and Fe(III) ions are present although raw materials contain only trivalent or divalent iron. The equilibrium between Fe(II) and Fe(III) depends on the atmosphere, melting temperature, time and composition of raw materials [25, 26]. Earlier molecular dynamics studies showed the ratio of divalent to trivalent iron not only

✉ Paweł Goj
  pgoj@agh.edu.pl

1   Faculty of Materials Science and Ceramics, AGH
     University of Science and Technology, ul. Mickiewicza 30,
     30-059 Kraków, Poland

affects the glass structure but also the glass properties, e.g., glass density [27–30].

The subject of the studies was the influence of Na_2O content on thermal properties of a glass of composition 30 Fe_2O_3–70 P_2O_5 mol%. This glass has good chemical and thermal properties and can incorporate to structure some external quantity of iron without the risk of crystallization.

Experimental

Polyphosphate glasses of the composition xNa_2O–(100–x) $(70P_2O_5$–$30Fe_2O_3)$ in mol% were prepared from chemical pure $NH_4H_2PO_4$, Fe_2O_3, and Na_2CO_3. Approximately 20 mass% overweight of $NH_4H_2PO_4$ was used to compensate P_2O_5 losses during the melting of the batch due to evaporation. Batches were melted for 2 h at 1473 K in Al_2O_3 crucible in an electric furnace with the furnace atmosphere as close to natural as possible. The tests were carried out on glass powder obtained by grinding in an agate mortar.

The chemical composition of the obtained glasses was checked by X-ray fluorescence (XRF). Samples for XRF were performed by pressed glass powder into thin tablets. The investigation has been carried out using Axios mAX WDXRF X-ray fluorescence spectrometer with Rh lamp of a power 4 kW (PANalytical). The analysis has been carried out with the use of the standardless method. The uncertainty of measurement was about 5%. The chemical composition of the obtained glasses was consistent with the assumption in the experimental uncertainty limit. All samples were XRD checked to be amorphous. The chemical compositions and the samples designations are shown in Table 1.

Glass transformation temperature T_g at the half of the heat capacity step on DSC curve, crystallization T_c as the onset of the first crystallization peak and melting T_m as the first melting peak maximum temperature was measured by differential scanning calorimetry (DSC) method combined with thermogravimetry (TG) at the heating rate 10 °C min^{-1}. Measurements were carried out using Netzsch STA 449 F5 Jupiter, operating in the heat flux DSC mode. Glass powder samples weighing 80 mg were heated in Al_2O_3 crucibles at a rate of 10 °C min^{-1} in a dry air atmosphere up to 1100 °C. Characteristic temperatures of the glass transformation effects and changes of specific heat at T_g were determined

by applying the Netzsch Proteus Thermal Analysis Program (version 5.0.0.).

Raman spectra were obtained using a LabRAM HR (HORIBA Jobin Yvon) spectrometer using the excitation wavelength of 532 nm. The diffraction grating was 1800 lines mm^{-1}. The spectra were recorded in point with the standard spot of about 1 μm.

Crystallization of the selected glasses (PFN0, PFN2 and PFN4 samples) was carried out at T_c temperature of exothermic DSC peak by 24 h. The phase composition of samples was investigated by X-ray diffractometry using Philips X'Pert pro diffractometer, and Cu $K_{\alpha1}$ radiation and measured spectra were analyzed using QualX software with POW_COD database [31].

Glass density was measured by a weighting of bulk glass samples in air and in water using the Archimedes method.

Results and discussion

The effect of content Na_2O in iron phosphate glass on its thermochemical properties is demonstrated by DSC curves. Figure 1 shows DSC curves for all the studied glasses. Transformation (T_g), crystallization (T_c), melting (T_m) temperatures, change in the specific heat capacity accompanying the glass transformation (ΔC_p), enthalpy of crystallization (ΔH), mass increase during crystallization (Δm) and glass stability criterions are summarized in Table 2.

All the samples show the characteristic for glasses transformation step at temperatures around 800 K and below. Figure 2 shows the effect of Na_2O content on the transformation temperature T_g and heat capacity ΔC_p accompanying the glass transformation. The transformation temperature decreases with increases in sodium content in the glass. The increasing content of Na leads to increase in the ΔC_p. The
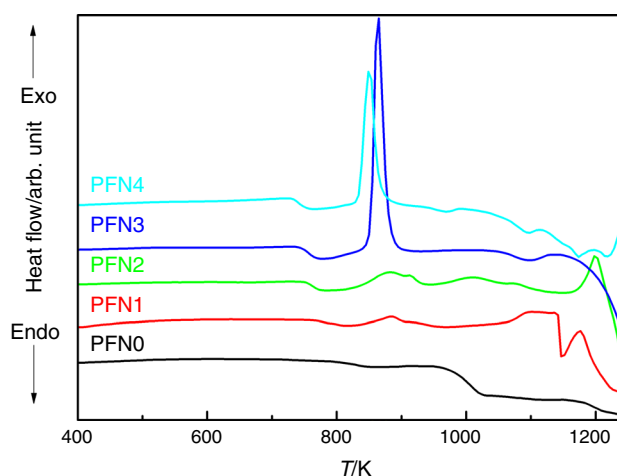
Table 1 Chemical composition of the glasses/mol%

Oxide	PFN0	PFN1	PFN2	PFN3	PFN4
P_2O_5	70	63	56	49	42
Fe_2O_3	30	27	24	21	18
Na_2O	0	10	20	30	40

Fig. 1 DSC curves of the studied glasses

Table 2 Transformation (T_g), crystallization (T_c), ΔC_p, mass increase during crystallization (Δm), melting temperature (T_m), crystallization enthalpy (ΔH), Angell parameter (K_A), Hruby parameter (K_H), Saad–Poulain parameter (K_{SP})
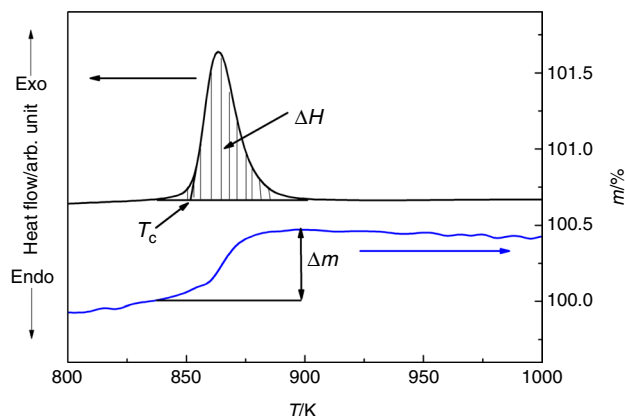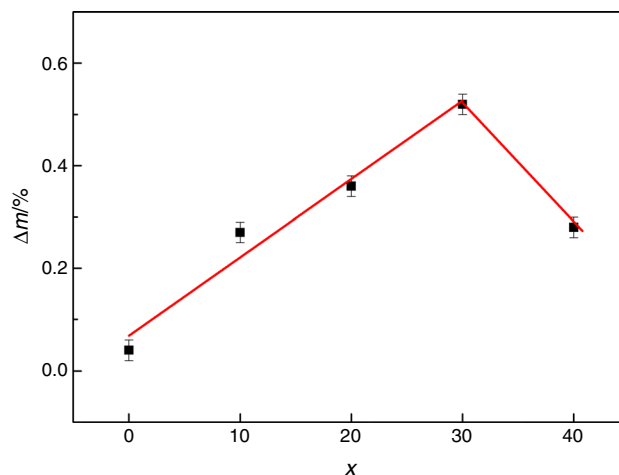
Na$_2$O content/mol%	T_g/K	ΔC_p/K	T_c/K	Δm/%	T_m/K	ΔH/J g^{-1}	K_A	K_H	K_{SP}
0	829(2)	0.133(9)	876(2)	0.04(2)	–	2.823(9)	47	–	2.27
10	786(2)	0.195(9)	838(2)	0.27(2)	1143(2)	12.93(9)	52	0.17	3.04
20	763(2)	0.311(9)	837(2)	0.36(2)	1083(2)	17.34(9)	74	0.30	4.56
30	755(2)	0.417(9)	853(2)	0.52(2)	1063(2)	159.7(9)	98	0.47	1.43
40	743(2)	0.496(9)	836(2)	0.28(2)	1081(2)	96.13(9)	93	0.38	1.88
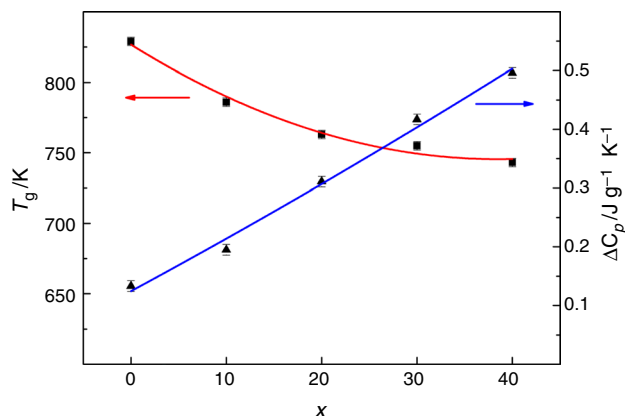
Fig. 2 Transformation temperature T_g and molar heat capacity ΔC_p accompanying the glass transformation as the Na$_2$O content (mol%)

Fig. 3 Section of DSC and TG curves with marked mass loss related to crystallization (Δm), crystallization temperature (T_c) and crystallization enthalpy (ΔH) for $x = 30$ glass

ΔC_p can be an indicator of a degree of the structural changes accompanying the glass transformation, and it is related to change in entropy [3, 32, 33].

At the higher temperatures, there is evidenced an exothermic effect of crystallization. In the case of the sodium-free sample, the effect is very little and hard to see. When the sodium content increases, the crystallization effect is being stronger. For the low Na$_2$O content samples, the effect is broad what may suggest a complex glass crystallization process. The most intense effect is observed for the PFN3 sample, and with further Na$_2$O increase in the glass, the crystallization effect seems to be less intense. After the peak, an endothermic effect is observed which may be due to melting or partial melting of the crystalline phases.

The crystallization enthalpy and mass increase during crystallization were determined from DSC and TG curves, respectively. Figure 3 shows exemplary mass change at crystallization temperature and ΔH as exothermic peak area for PFN3 glass. The mass changes at the crystallization temperature for all the glasses are presented in Table 2. The change increases with increasing content of Na$_2$O up to 30 mol% and then decreases (Fig. 4). In the studied glass system, there were observed previously mass losses during the release of absorbed water or evaporation of P$_2$O$_5$ at temperatures above 1300 K [15]. Here, we observe the opposite effect of small mass increase. One of the possible explanations of the effect

Fig. 4 Mass increase during the crystallization

may be related to the change in iron oxidation state from Fe(II) to Fe(III) during the crystallization. The change leads to an increase in the electric charge of the system which needs to be compensated by the absorption of oxygen anions. Nevertheless, this is only an assumption that needs further studies. A similar manner has a change in the ΔH with increasing content of Na$_2$O in the glass. The more intense

exothermic effect can be related to the more intense crystallization of phases containing Fe(III). That would explain the correlation between ΔH and Δm. Also, the rapid growth of crystallization enthalpy about 30 mol% could suggest a change in the crystallization mechanism.

The thermal stability is an important parameter in the case of waste vitrification [3]. The glass stability was evaluated using Hruby (K_H), Angell (K_A) and Saad–Poulain (K_{SP}) parameters [34, 35]. Higher values of these parameters mean greater its stability of the crystallization. These parameters have the following formulas:

$$K_H = \frac{T_c - T_g}{T_m - T_c} \tag{1}$$

$$K_A = T_c - T_g \tag{2}$$

$$K_{SP} = \frac{(T_C - T_g)(T_c^{max} - T_c)}{T_g} \tag{3}$$

where T_c is the onset temperature of crystallization, T_c^{max} is the peak of crystallization maximum temperature of, T_g is transformation temperature, and T_m is the melting temperature.

Depending on a parameter used, the results may vary. The Angell parameter is the very simple difference between crystallization and transformation temperature. Hruby's and Saad–Poulain parameters are more complex and contain other relations affecting glass-forming tendency. The obtained glass stability parameters are summarized in Table 1. The investigated glasses have good thermal stability comparable with silicate glasses (K_H values from 0.14 to 1.3) [23, 24, 34], and these values are very similar to iron phosphate glasses of ratio Fe/P = 2/3 [3]. According to Angell parameter, glass stability increases with increasing sodium content. The case of Hruby's parameter is different because of the difference between melting and crystallization temperature. The melting temperature decreases with increasing Na_2O content to 30 mol% and then increase it has an influence on glass stability. The greater difference between melting and crystallization temperature glass stability is weaker. The Saad–Poulain parameter increases to 20 mol% ($K_{SP} = 4.56$), and above this value, it rapidly falls.

The density and molar volume for glasses as a function of Na_2O content are shown in Fig. 5. The changes in density and molar volume are not continuous. The density increases to about 20 mol% and then decreases. Also, the molar volume does not decrease continuously. The above value, 20 mol% of sodium oxide, decreases more slowly. Similar behavior of glass density was reported earlier for glasses with molar ratio Fe/P = 2/3 [3]. It can be explained as the effect of higher than 20 mol% Na_2O content stabilizing
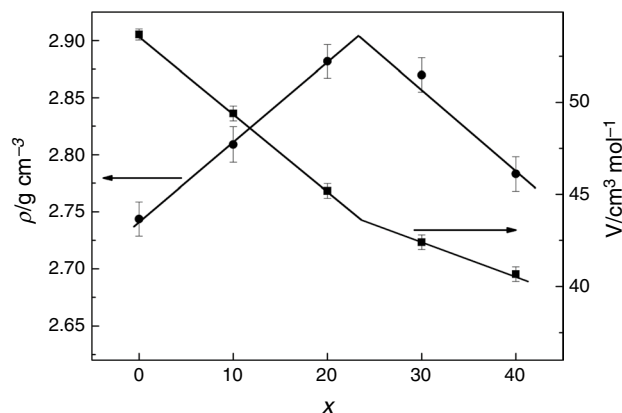

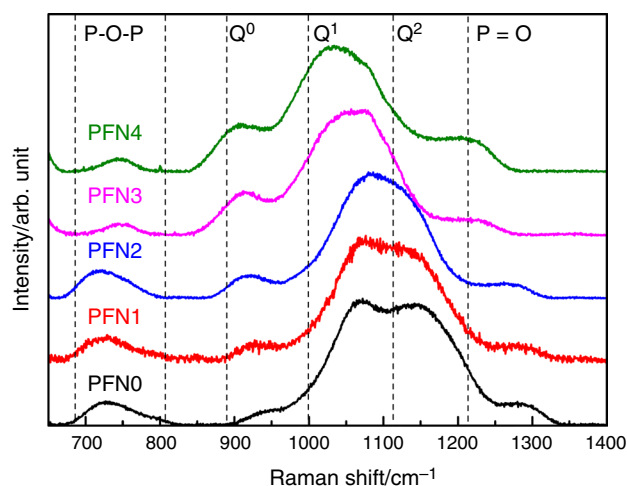**Fig. 5** Density and molar volume as Na_2O content

Fig. 6 Raman spectra of glasses

Fe(III) and oxidizing partially divalent iron. Earlier experimental studies [36] show a correlation between glass density, divalent iron and sodium content for glasses of Fe/P = 2/3. Increasing the content of Na_2O causes an increase in Fe(II) quantity and densification of glass. Then, 30 mol% Na_2O causes a decrease of Fe(II) content and glass density. Also, earlier molecular dynamic simulations show that increasing the content of Fe(II) in glass causes the densification of a glass network [30].

Figure 6 shows the obtained Raman spectra of studied glasses. Iron phosphate glasses are characterized by intense broadbands in range of 850–1400 cm^{-1} associated with vibrations of P–O bonds in Q^i structural units. In Q^i notation, Q means [PO_4] tetrahedra and i is the number of bridging oxygens of this tetrahedra. The band about 1300 cm^{-1} is related to stretching vibrations of the P=O bond [37]. The strong band about 1160 cm^{-1} is related to the symmetric stretching vibrations of non-bridging oxygens in Q^2 structural units. Two bands about 1090 and 930 cm^{-1} are assigned

to symmetric stretching vibrations of non-bridging oxygens in Q^1 and Q^0, respectively. The bands in the range from 700 to 800 cm^{-1} are related to vibrations of P–O–P linkages [37–39]. The intensity of band related to Q^2 decreases, Q^0 increases, and Q^1 rather remains unchanged. Also, the intensity of bands related to P–O–P linkages decreases. These changes suggest the depolymerization of glass. The quantity of Q^0 increases at the expense of Q^2. Furthermore, the band related to Q^1 structural unit moves toward lower values of Raman shift from 1070 to 1030 cm^{-1}. The band related to symmetric stretching vibrations of non-bridging oxygens in Q^1 connected to Fe should be about 1050–1140 cm^{-1} [14, 38, 39]. This shift can, therefore, be associated with a decrease in Q^1-Fe connections.

Crystallization of PFN0, PFN2 and PFN4 glasses was carried out. Figure 7 shows XRD patterns of glasses after crystallization. In the case of the PFN0 glass, crystallization was not observed. The DSC curve for this glass shows that the exothermic effect of crystallization is very small ($\Delta H = 2.823(9)$ J g^{-1}). It is possible that crystallization, in this case, is very slow and time of crystallization was not enough. Compounds crystallizing in the investigated glasses and their semi-quantity analysis are summarized in Table 3. In the PFN2, glass crystallizes mainly NaFeP$_2$O$_7$ and some FePO$_4$. The ratio of Na/Fe in NaFe^{3+}P$_2$O$_7$ phase is very similar to this ratio in the glass. The little excess of Fe makes the possible formation of FePO$_4$. The XRD pattern of PFN4 crystallized sample is more complex. In this case, the three crystallized phases are Na$_4$Fe$_2^{2+}$(P$_2$O$_7$)$_2$, Na$_7$Fe$_3^{3+}$(P$_2$O$_7$)$_4$ and Na$_7$Fe$_4^{3+}$P$_9$O$_{32}$. Similarly, in this case, Na/Fe ratio in the crystalline and in the amorphous phase is comparable. This may indicate that complex phases consist of many elements that crystallize easier. It can be seen that the crystal phases containing Fe(III) are preferred in the glasses after

Fig. 7 XRD patterns of PFN0, PFN2 and PFN4 glasses after crystallization

Table 3 Compounds crystallizing in the investigated glasses, semi-quantity analysis and POW_COD reference ID

Sample	Crystal phase	Semi-quantity/ mass%	COD ID
PFN0	–	–	–
PFN2	FePO$_4$	16.0	00-600-0577
	NaFeP$_2$O$_7$	84.0	00-154-5058
PFN4	NaFeP$_2$O$_7$	17.9	00-154-5058
	Na$_3$Fe$_2$P$_3$O$_{12}$	9.4	00-153-3686
	Na$_7$Fe$_4$P$_9$O$_{32}$	31.1	00-153-0646
	Na$_4$Fe$_2$(P$_2$O$_7$)$_2$	26.8	00-400-1802
	Na$_7$Fe$_3$(P$_2$O$_7$)$_4$	31.1	00-154-5022

crystallization. It is consistent with the mass increase at crystallization and transformation of Fe(II) to Fe(III). This supports the idea of the relation of the mass increase with the change in iron redox state. Generally, Fe(III) content in iron phosphate glass ceramics depends on the atmosphere, composition of glass and heat treatment [3]. Phases formed in the investigated glasses are similar to phases observed in previous investigations of cesium [40] and sodium iron phosphate glasses [3, 9, 41].

The main crystallization product of PFN2 is NaFeP$_2$O$_7$. In this phase, these are P$_2$O$_7$ dimers connected to each other by Fe^{3+} octahedrons [42]. The monoclinic FePO$_4$ is built of separated [PO$_4$] tetrahedra connected to each other by Fe of 5 coordination to oxygen. The glass can have an iron with coordination to oxygen from 4 to 6 [28, 39, 41, 43, 44]. The phase composition indicates that glasses of 20 mol% Na$_2$O can have structure of isolated [PO$_4$] tetrahedra and P$_2$O$_7$ dimers connected to each to other by Fe polyhedra, but always at least three oxygens of [PO$_4$] are connected to Fe or P. In case of PFN4 sample crystallization products also have [PO$_4$] tetrahedra and P$_2$O$_7$ dimers but [PO$_4$] tetrahedra can be connected to other P or Fe by less than three oxygens [45–48]. Increasing Na$_2$O content causes depolymerization of the glass network. The structure of the glass of composition higher than 20 mol% can be more open and also have the P$_2$O$_7$ dimers and isolated [PO$_4$] tetrahedra, but the quantity of Fe–O–P and P–O–P bridges decreases. The structural changes are connected with ΔC_p changes. The sodium into glass structure breaks network oxide bridges (Fe–O–P and P–O–P bridges), and a number of unidirectional Na–O bounds increase. The network glass becomes more open, flexible and easier to reorganize. It may explain the ΔC_p increase and T_g decrease with sodium content.

The nonlinear changes of glass density, molar volume, Δm and ΔH at 30 mol% Na$_2$O suggest structural rebuilding. It is likely that the quantity of Fe(II) is the highest at the turning point (30 mol% Na$_2$O) and then decrease. Also, changes in these properties are related to changes in the iron
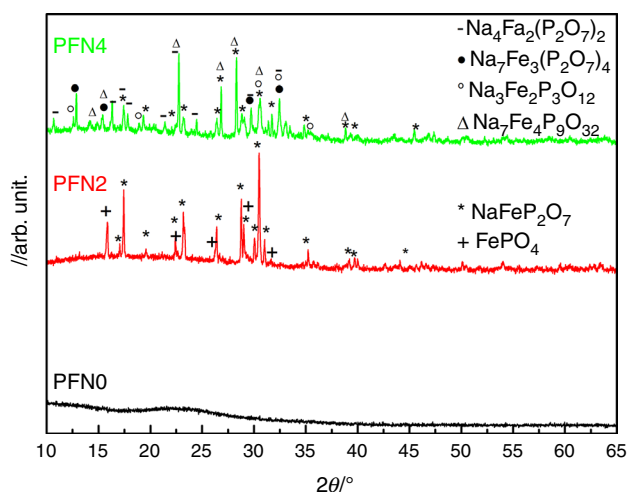
coordination number to oxygen. Previous molecular dynamics simulations show that increasing the content of Fe(II) increases the average coordination number of Fe [30]. Also, a similar influence has increasing content of Na_2O up to 20 mol% for glasses of Fe/P = 2/3 then average coordination number decrease [43].

Conclusions

The thermal properties of 30% Fe_2O_3–70% P_2O_5 mol% glass with increasing Na_2O content were investigated. The investigated glasses have low transformation and melting temperatures and better thermal stability than silicate glasses. Increasing the content of sodium causes depolarization of the iron phosphate glass network. The quantity of linkages between phosphate tetrahedra and iron polyhedra falls with increasing sodium content. This affects gradual changes in thermal properties.

Similar to glasses of Fe/P = 2/3, tested glasses exhibit phosphate anomaly, which means the discontinuous change in some properties. Nonlinear changes of density, molar volume and crystallization enthalpy with increasing content of Na_2O are present for tested glass. The crystallization products and mass changes during crystallization suggest changes in short-range ordering around iron together with changes in iron oxidation.

References

1. Joseph K, Stennett MC, Hyatt NC, Asuvathraman R, Dube CL, Gandy AS, et al. Iron phosphate glasses: bulk properties and atomic scale structure. J Nucl Mater. 2017;494:342–53.
2. Huang W, Day DE, Ray CS, Kim CW. High temperature properties of an iron phosphate melt containing high chrome nuclear waste. J Nucl Mater. 2005;346:298–305.
3. Stoch P, Ciecinska M, Stoch A. Thermal properties of phosphate glasses for salt waste immobilization. J Therm Anal Calorim. 2014;117:197–204.
4. Donald IW. Waste immobilization in glass and ceramic based hosts. New York: Wiley; 2010.
5. Bingham PA, Hand RJ, Scales CR. Immobilization of simulated plutonium-contaminated material in phosphate glass: an initial scoping study. Mater Res Soc Symp Proc. 2006;932:345–52.
6. Simon V, Chiuzbăian SG, Neumann M, Eniu D, Indrea E, Török-kiss A, et al. Photoelectron spectroscopy on iron-containing CaO–SiO_2–P_2O_5 glass ceramics. Mod Phys Lett B. 2000;14:767–72.
7. Lin ST, Krebs SL, Kadiyala S, Leong KW, LaCourse WC, Kumar B. Development of bioabsorbable glass fibres. Biomaterials. 1994;15:1057–61.
8. Majhi MR, Kumar R, Singh SP, Pyare R. Physico-chemical properties and characterization of CaO–Fe_2O_3–P_2O_5 glass as a bioactive ceramic material. J Biomim Biomater Tissue Eng. 2011;12:1–24.
9. Ciecińska M, Stoch P, Stoch A, Nocuń M. Thermal properties of $60P_2O_5$–$20Fe_2O_3$–$20Al_2O_3$ glass for salt waste immobilization. J Therm Anal Calorim. 2015;121:1225–32.
10. Ojovan MI, Batyukhnova OG. Glasses for nuclear waste immobilization. In: WM'07 conference; 2007. p. 15.
11. Ojovan MI, Lee WE. Glassy wasteforms for nuclear waste immobilization. Metall Mater Trans A Phys Metall Mater Sci. 2011;42:837–51.
12. Ojovan MI, Lee WE. An introduction to nuclear waste immobilisation.
13. Yu X, Day DE, Long GJ, Brow RK. Properties and structure of sodium–iron phosphate glasses. J Non Cryst Solids. 1997;215:21–31.
14. Goj P, Jeleń P, Marczewska B, Stoch P. Effect of β-Irradiation on the structure of iron polyphosphate glass. J Nucl Mater. 2019;523:198–205.
15. Ciecińska M, Goj P, Stoch A, Stoch P. Thermal properties of $60P_2O_5$–$(40-x)Al_2O_3$–xNa_2O glasses. J Therm Anal Calorim. 2020;139:1763–1769.
16. Greaves GN, Gurman SJ, Gladden LF, Spence CA, Cox P, Sales BC, et al. A structural basis for the corrosion resistance of lead-iron-phosphate glasses: an X-ray absorption spectroscopy study. Philos Mag B. 1988;58:271–83.
17. Musinu A, Piccaluga G, Pinna G. Structural properties of lead-iron phosphate glasses by X-ray diffraction. J Non Cryst Solids. 1990;122:52–8.
18. Zhang L, Brow RK, Schlesinger ME, Ghussn L, Zanotto ED. Glass formation from iron-rich phosphate melts. J Non Cryst Solids. 2010;356:1252–7.
19. Stoch P, Ciecinska M. Thermochemistry of phosphate glasses for immobilization of dangerous waste. J Therm Anal Calorim. 2012;108:705–9.
20. Kim C-W, Day DE. Immobilization of Hanford LAW in iron phosphate glasses. J Non Cryst Solids. 2003;331:20–31.
21. Zhang L, Ghussn L, Schmitt ML, Zanotto ED, Brow RK, Schlesinger ME. Thermal stability of glasses from the $Fe_4(P_2O_7)_3$–$Fe(PO_3)_3$ system. J Non Cryst Solids. 2010;356:2965–8.
22. Ma L, Brow RK, Ghussn L, Schlesinger ME. Thermal stability of Na_2O–FeO–Fe_2O_3–P_2O_5 glasses. J Non Cryst Solids. 2015;409:131–8.
23. Cabral AA, Cardoso AAD, Zanotto ED. Glass-forming ability versus stability of silicate glasses. I. Experimental test. J Non Cryst Solids. 2003;320:1–8.
24. Lin SE, Cheng YR, Wei WCJJ. Synthesis and long-term test of borosilicate-based sealing glass for solid oxide fuel cells. J Eur Ceram Soc. 2011;31:1975–85.
25. Ray CS, Fang X, Karabulut M, Marasinghe GK, Day DE. Effect of melting temperature and time on iron valence and

crystallization of iron phosphate glasses. J Non Cryst Solids. 1999;249:1–16.

26. Marasinghe GK, Karabulut M, Ray CS, Day DE, Shumsky MG, Yelon WB, et al. Structural features of iron phosphate glasses. J Non Cryst Solids. 1997;222:144–52.

27. Jolley K, Smith R. Iron phosphate glasses: structure determination and radiation tolerance. Nucl Instrum Methods Phys Res Sect B Beam Interact Mater Atoms. 2016;374:8–13.

28. Joseph K, Jolley K, Smith R. Iron phosphate glasses: structure determination and displacement energy thresholds, using a fixed charge potential model. J Non Cryst Solids. 2015;411:137–44.

29. Al-Hasni B, Mountjoy G. Structural investigation of iron phosphate glasses using molecular dynamics simulation. J Non Cryst Solids. 2011;357:2775–9.

30. Goj P, Stoch P. Molecular dynamics simulations of P$_2$O$_5$–Fe$_2$O$_3$–FeO glass system. Ceram Mater. 2018;70:102–15.

31. Altomare A, Corriero N, Cuocci C, Falcicchio A, Moliterni A, Rizzi R. QUALX2.0: a qualitative phase analysis software using the freely available database POW-COD. J Appl Crystallogr Int Union Crystallogr. 2015;48:598–603.

32. Stoch L, Wacławska I, Środa M. Thermal study of the influence of chemical bond ionicity on the glass transformation in (Na$_2$O, CaO, MgO)–Al$_2$O$_3$–SiO$_2$ glasses. J Therm Anal Calorim. 2004;77:57–63.

33. Stoch A. Thermochemistry of solids with flexible structures. J Therm Anal Calorim. 1998;54:9–24.

34. Nascimento MLF, Souza LA, Ferreira EB, Zanotto ED. Can glass stability parameters infer glass forming ability? J Non Cryst Solids. 2005;351:3296–308.

35. Hruby A. Evaluation of glass-forming tendency by means of DTA. Czechoslov J Phys. 1972;22:1187–93.

36. Bingham PA, Hand RJ, Hannant OM, Forder SD, Kilcoyne SH. Effects of modifier additions on the thermal properties, chemical durability, oxidation state and structure of iron phosphate glasses. J Non Cryst Solids. 2009;355:1526–38.

37. Yadav AK, Singh P. A review of the structures of oxide glasses by Raman spectroscopy. RSC Adv. 2015;5:67583–609.

38. Stoch P, Goj P, Ciecińska M, Stoch A. Structural features of 19Al$_2$O$_3$–19Fe$_2$O$_3$–62P$_2$O$_5$ glass from a theoretical and experimental point of view. J Non Cryst Solids. 2019;521:119499.

39. Stoch P, Stoch A, Ciecinska M, Krakowiak I, Sitarz M. Structure of phosphate and iron-phosphate glasses by DFT calculations and FTIR/Raman spectroscopy. J Non Cryst Solids. 2016;450:48–60.

40. Joseph K, Ghosh S, Govindan Kutty KV, Vasudeva Rao PR. Crystallization kinetics, stability and glass forming ability of iron phosphate and cesium loaded iron phosphate glasses. J Nucl Mater. 2012;426:233–9.

41. Stoch P, Szczerba W, Bodnar W, Ciecinska M, Stoch A, Burkel E. Structural properties of iron-phosphate glasses: spectroscopic studies and ab initio simulations. Phys Chem Chem Phys. 2014;16:19917–27.

42. Moya-Pizarro T, Salmon R, Fournes L, Le Flem G, Wanklyn B, Hagenmuller P. Etudes cristallographiques magnetique et par resonance Mossbauer de la variete de haute temperature du pyrophosphate NaFeP$_2$O$_7$. J Solid State Chem. 1984;53:387.

43. Goj P, Stoch P. Molecular dynamics simulations of P$_2$O$_5$–Fe$_2$O$_3$–FeO–Na$_2$O glasses. J Non Cryst Solids. 2018;500:70–7.

44. Jolley K, Smith R. Radiation tolerance of iron phosphate: a study of amorphous and crystalline structures. J Nucl Mater. 2016;479:347–56.

45. Barpanda P, Liu G, Ling CD, Tamaru M, Avdeev M, Chung S-CC, et al. Na$_2$FeP$_2$O$_7$: a safe cathode for rechargeable sodium-ion batteries. Chem Mater. 2013;25:3480.

46. Masquelier C, d Yvoire F, Rodier N. Crystal structure of the sodium ion conductor alpha-Na$_7$Fe$_3$(P$_2$O$_7$)$_4$: evidence for a long-range ordering of the Na$^+$ ions. J Solid State Chem. 1991;95:156.

47. Belokoneva EL, Ruchkina EA, Dimitrova OV, Stefanovich SY. Synthesis and crystal structure of a new trigonal modification of Na$_3$Fe$_2$(PO$_4$)$_3$. Zhurnal Neorg Khimii. 2002;47:1423–6.

48. Rochere M, Kahn A, D'Yvoire F, Bretey E. Crystal structure and cation transport properties of the ortho-diphosphates Na7(MP2O7)4PO4 (M = Al, Cr, Fe). Mater Res Bull. 1985;20:27.